1 Revision 3

## Hydrous wadsleyite crystal structure up to 32 GPa

3 Word count: 8621

2

5

12

14

15

16

17

18

19

20

21

22

23

24

25

26

- 4 Fei Wang<sup>a,b</sup>, Elizabeth C. Thompson<sup>c</sup>, Dongzhou Zhang<sup>d</sup>, Jingui Xu<sup>d</sup>, Ercan E. Alp<sup>e</sup>, Steven D. Jacobsen<sup>a</sup>
- 6 a Department of Earth and Planetary Sciences, Northwestern University, Evanston, IL 60208, USA
- 7 Bayerisches Geoinstitut, University of Bayreuth, Bayreuth, Germany
- 8 CDepartment of Earth and Environmental Systems, The University of the South, Sewanee, TN 37383, USA
- 9 d Hawai'i Institute of Geophysics and Planetology, School of Ocean and Earth Science and Technology,
- 10 University of Hawai'i at Manoa, Honolulu, HI 96822
- 11 <sup>e</sup>Advanced Photon Source, Argonne National Laboratory, Argonne, IL 60439 USA
- 13 Corresponding author: Fei Wang (<u>feiwang2020@u.northwestern.edu</u>)

### Abstract

Hydroxylation of wadsleyite, β-(Mg,Fe)<sub>2</sub>SiO<sub>4</sub>, is associated with divalent cation defects and well known to affect its physical properties. However, an atomic-scale understanding of the defect structure and hydrogen bonding at high pressures is needed to interpret the influence of water on the behavior of wadsleyite in the mantle transition zone. We have determined the pressure evolution of the wadsleyite crystal symmetry and structure, including all O...O interatomic distances, up to 32 GPa using single-crystal X-ray diffraction on two well-characterized, Fe-bearing (Fo<sub>90</sub>) samples containing 0.25(4) and 2.0(2) wt% H<sub>2</sub>O. Both compositions undergo a pressure-dependent monoclinic distortion from orthorhombic symmetry above 9 GPa, with the less hydrous sample showing a larger increase in distortion at increased pressures due to the difference in compressibility of the split M3 site in the monoclinic setting arising from preferred vacancy ordering at the M3B site. Although hydrogen positions cannot be modeled from the X-ray diffraction data, the pressure evolution of the longer O1...O4 distance

in the structure characterizes the primary hydrogen bond length. We observe the hydrogen-bonded O1...O4 distance shorten gradually from 3.080(1) Å at ambient pressure to about 2.90(1) Å at 25 GPa, being still much longer than is defined as strong hydrogen bonding (2.5–2.7 Å). Above 25 GPa and up to the maximum pressure of the experiment at 32.5 GPa, the hydrogen-bonded O1...O4 distance decreases no further, despite the fact that previous spectroscopic studies have shown that the primary O–H stretching frequencies continuously drop into the regime of strong hydrogen bonding (<3200 cm<sup>-1</sup>) above ~15 GPa. We propose that the primary O1–H...O4 hydrogen bond in wadsleyite becomes highly non-linear at high pressures based on its deviation from frequency-distance correlations for linear hydrogen bonds. One possible explanation is that the hydrogen position shifts from being nearly on the long O1–O4 edge of the M3 site to a position more above O1 along the *c*-axis.

Keywords: Wadsleyite, mantle transition zone, hydrogen bond, water

40 Introduction

The nominally anhydrous minerals (NAMs) wadsleyite and ringwoodite can incorporate 1–2 wt% H<sub>2</sub>O into their crystal structures as hydroxyl groups at the elevated pressures and temperatures of the Earth's mantle transition zone (e.g., Smyth 1987; Fei and Katsura 2020), which suggests that the Earth's mantle could play a dynamic role in the evolution of surface water reservoirs over geologic time (Dong et al. 2021). Although no samples of terrestrial wadsleyite have been reported, the recent discovery of hydrous ringwoodite containing ~1.5 wt% water, found as a natural inclusion in a diamond (Pearson et al. 2014), provides evidence that the transition zone is locally hydrated. Mapping regional-scale hydration from seismological data (e.g., Karato 2011; Wang et al. 2018) requires knowledge of the effects of hydration on the physical properties of NAMs at transition zone pressures and temperatures. For example, theory and experiments show that the incorporation of even small quantities of H<sub>2</sub>O significantly influence the elastic properties of wadsleyite governing the velocity of seismic waves (e.g., Tsuchiya and

Tsuchiya 2009; Mao et al. 2011; Buchen et al. 2018; Gwanmesia et al. 2020). As the elastic properties of Earth materials are ultimately controlled by interatomic potentials, knowledge of the crystal structure and evolution of hydrogen bonding in wadsleyite is useful in predicting the physical properties expected for hydrous and anhydrous regions of the upper transition zone.

The crystal structure of wadsleyite is unique among the Mg<sub>2</sub>SiO<sub>4</sub> polymorphs in possessing a sorosilicate group (Si<sub>2</sub>O<sub>7</sub>). The structure consists of three octahedral metal cation sites (M) occupied by Mg<sup>2+</sup>, Fe<sup>2+</sup> or Fe<sup>3+</sup>, one tetrahedral site (T) occupied by Si<sup>4+</sup> or Fe<sup>3+</sup>, and four distinct oxygen sites (Horiuchi & Sawamoto 1981, Smyth et al. 1997) (Figure S1). The first step in understanding the impacts of hydration on the physical and mechanical properties of wadsleyite and other NAMs is determining where hydrogen is structurally accommodated and charge-balanced by associated cation defect vacancies. Smyth et al. (1987) recognized that the O1 site of wadsleyite is a favorable location for H based on the electrostatic potential as this site is coordinated to five Mg sites but no Si, and is therefore under-bonded. Shortly thereafter, McMillan et al. (1991) observed OH absorption bands in wadsleyite using Fourier transform infrared (FTIR) spectroscopy on wadsleyite crystals that had been fortuitously hydrated during synthesis by dehydration of the pyrophyllite pressure medium.

The pleochroic behavior of OH absorbance observed in polarized FTIR spectra (Jacobsen et al. 2005) showed that the primary OH bands at 3300–3400 cm<sup>-1</sup> can be explained by H at the O1 site, with protonation of the unshared O1–O4 edge of the M3 site, where most cation vacancies were observed. Jacobsen et al. (2005) also noted that some protonation may occur along the shorter O1–O4 edge of the M3 site that is shared with the M2 site, as well as possibly along the O1–O3 edge of the M3 site. Similar sites were proposed from room-pressure XRD and high-pressure FTIR spectroscopy measurements by Dion et al. (2010). Sano-Furukawa et al. (2011) refined the H positions in wadsleyite using powder neutron diffraction data and confirmed that the dominant hydrogen site is located close to O1 and along the longer of the two distinct O1–O4 edges of the M3 site, with minor occupation along the O1–O3 edge of the M3 site. Using single-crystal neutron diffraction data, Purevjav et al. (2016) confirmed that the major H site is along the longer and unshared O1–O4 edges of the M3 site with an O–H distance of ~1 Å

and slightly non-linear hydrogen bond angle of 171°. Whereas the longer O1–O4 edges of M3 site appear to host the majority of H in wadsleyite, realistically there are also many minor sites, as evidenced by up to 15 observed O–H stretching frequencies, which can tentatively be assigned to other sites in the structure based on frequency-distance correlations (Libowitzky, 1999; Kohn et al. 2002).

In silicates and oxides, hydrogen bonds form when a hydrogen atom, bonded to a donor oxygen atom via a polar covalent bond, interacts electrostatically with a nearby acceptor oxygen (Emsley 1981). Hydrogen bonds have both a characteristic bond length, d(O...O), defined by the distance between the donor and acceptor oxygen atoms along O–H...O, and a characteristic O–H stretching frequency, which is corelated to hydrogen-bond strength, assuming the hydrogen bond angle along O–H...O is close to 180° (Libowitzky, 1999). Typically, hydrogen bonds form an asymmetric potential well between donor and acceptor oxygen atoms, where the O–H bond is shorter than the H...O distance. Although hydrogen bonds in minerals have a poorly defined upper limit beyond  $\sim$ 3 Å, strong hydrogen bonds are defined as having d(O...O) of 2.5–2.7 Å (Libowitzky, 1999). On compression, if d(O...O) shortens, the O–H bond lengthens due to the increased attractive force of the acceptor oxygen, weakening the O–H bond and lowering the O–H stretching frequency (Libowitzky 1999). Whereas the O–H stretching frequencies in most hydrous minerals are observed at 3200–4000 cm<sup>-1</sup>, strong hydrogen bonds have stretching frequencies in the range of 1600–3200 cm<sup>-1</sup>.

High-pressure FTIR spectroscopy studies of wadsleyite have shown that the primary O–H stretching bands associated with hydrogen bonding along the O1–O4 edge at 3300–3400 cm<sup>-1</sup> shift strongly with increasing pressure to lower frequencies of about 3150–3250 cm<sup>-1</sup> at 16–18 GPa, the maximum pressure of those experiments (Deon et al. 2010; Yang et al. 2014). This is consistent with earlier findings of Kleppe et al. (2006), who reported Raman spectroscopy measurements of hydrous Febearing wadsleyite up to approximately 50 GPa and found that the 3300-3400 cm<sup>-1</sup> band became a very broad and weak feature at frequencies below 3000 cm<sup>-1</sup> above approximately 40 GPa. Because O–H stretching frequencies in hydrous wadsleyite drop below ~3200 cm<sup>-1</sup> above 15 GPa, they enter the regime of strong hydrogen bonding as defined for linear hydrogen bonds (Libowitzky 1999). Since the primary

hydrogen bond in wadsleyite, O1–H...O4, is rather long at room pressure with d(O1...O4) = 3.1 Å (Jacobsen et al. 2005), a decrease of O–H stretching frequencies to below 3200 cm<sup>-1</sup> above 15 GPa would imply a drastic compression of the O1–O4 edge if the hydrogen bond remains fairly linear. One objective of this study is to determine all the interatomic O...O distances in the wadsleyite structure up to 32 GPa in part to test whether or not spectroscopic indications of O–H stretching frequencies below ~3200 cm<sup>-1</sup> are consistent with conventionally defined strong hydrogen bonds with d(O...O) < 2.7 Å.

Another consequence of the hydration of wadsleyite is a change in symmetry from orthorhombic (Imma) to monoclinic (I2/m), which is defined by the deviation of the unit-cell  $\beta$ -angle from 90.0°. This was first recognized by Smyth et al. (1997) and subsequently observed, to varying degrees, by other studies (e.g., Jacobsen et al. 2005; Holl et al. 2008). The breaking of orthorhombic symmetry in hydrous wadsleyite is believed to result from the unequal distribution of vacancies at M3 sites, resulting in two non-equivalent M3A and M3B sites (Smyth et al. 1997). A Raman spectroscopy study of Fe-bearing wadsleyite with 2.4 wt% water by Kleppe et al. (2006) inferred monoclinic symmetry at high pressure and suggested, based on Raman spectra, that the monoclinic angle might increase with pressure. In contrast, Holl et al. (2008) evaluated the  $\beta$ -angle in wadsleyite containing 1.66 wt% H<sub>2</sub>O up to 10 GPa but did not observe a pressure-induced change in  $\beta$ -angle. Determining the structure and symmetry of hydrous wadsleyite at pressures exceeding 10 GPa is necessary to more adequately understand the physical properties of hydrous wadsleyite in the transition zone.

To date, only one experimental study (Hazen et al. 2000) has examined the structure of wadsleyite at high pressures ( $P_{\text{max}} = 10.1 \text{ GPa}$ ) from single-crystal X-ray diffraction data, but the water content of the samples in that study was not determined. Therefore, we have undertaken high-precision structure refinements of well-characterized hydrous wadsleyite single crystals under quasi-hydrostatic compression up to 35 GPa. To directly compare the effects of water, one sample contains ~2.0 wt% H<sub>2</sub>O while the other sample contains ~0.25 wt% H<sub>2</sub>O. Both samples approximate the Fe-content of mantle olivine (Fo<sub>90</sub>). Our two main objectives are: (1) evaluate the crystal symmetry evolution with pressure, and (2) determine the pressure-dependence of all interatomic O...O distances in the structure to compare

hydrogen-bonded versus non-hydrogen bonded O-O edges for comparison to previously observed O-H stretching frequencies at high pressures. The results of this study help to explain the modified physical properties of hydrous wadsleyite in the transition zone.

#### Materials and Methods

### Sample synthesis and characterization

130

131

132

133

134

135

136

137

138

139

140

141

142

143

144

145

146

147

148

149

150

151

152

153

This study examines two different hydrous Fe-bearing wadsleyite samples from synthesis run Z0570 containing 2.0(2) wt%  $H_2O$  and from run Z0902 containing 0.25(4) wt%  $H_2O$  (Chang et al. 2015). Both samples were synthesized using the 5000-ton, multi-anvil press at Bayerisches Geoinstitut, University of Bayreuth, Germany. For run Z0570, starting materials of San Carlos olivine plus liquid water were welded into a Pt capsule, compressed to 18 GPa and heated to a peak temperature of 1400 °C for several minutes before annealing at 1100 °C for 30 minutes. Run products from Z0570 consisted of both wadsleyite and ringwoodite. For run Z0902, San Carlos olivine was used without the addition of water and compressed to 11 GPa for annealing at 1100 °C (Chang et al. 2015). No phase other than wadsleyite was observed in the run product of Z0902. Electron microprobe analyses give values of  $Mg/(Mg+\Sigma Fe)$  of 0.89 and 0.90 for run Z0570 and run Z0902, respectively (Chang et al. 2015). FTIR spectra for both samples are presented in Chang et al. (2015) and indicate 1.4 wt% H<sub>2</sub>O and 0.25 wt% H<sub>2</sub>O in run Z0570 and Z0902, respectively, using the calibration of Deon et al. (2010). The water content of Z0570 was also measured at two secondary ion mass spectrometry laboratories by Chang et al. (2015), resulting in 1.93(22) wt% H<sub>2</sub>O and 2.07(24) wt% H<sub>2</sub>O. Since FTIR methods are less reliable for very high water contents in wadsleyite, we used 2.0(2) wt% H<sub>2</sub>O for the more hydrous sample (Z0570) and 0.25(4) wt%  $H_2O$  for the less hydrous sample (Z0902).

# Synchrotron Mössbauer Spectroscopy

To determine the oxidation states of iron, time-domain synchrotron Mössbauer spectroscopy (SMS) was conducted on beamline 3-ID-B of the Advanced Photon Source (APS), Argonne National Laboratory. One ~150 μm diameter grain was selected from each synthesis run. A Si (111) double crystal monochromator and a 4-bounce inline high-resolution monochromator (Toellner 2000) was used to filter the X-ray energy to a bandwidth of 1 meV at 14.4125 keV. The monochromatic X-rays were focused into a 15 μm diameter beam using a Kirkpatrick-Baez type mirror. The nuclear delay signal was recorded in the 21–128 ns time window between the X-ray pulses generated by the synchrotron. Time-domain Mössbauer spectra were fit using CONUSS 2.2.0 (Sturhahn, 2000) to get the hyperfine parameters of Fe and the ferric-to-ferrous ratio for each sample. A two-doublet model was used to fit each spectrum, with one doublet each for Fe<sup>2+</sup> and Fe<sup>3+</sup>, as it gave the best statistical fit. The isomer shift of Fe<sup>2+</sup> was fixed at 1.04 mm/s relative to stainless steel based on previous Mössbauer data (Chang et al. 2015).

### Sample loading environment and pressure determination

High pressures were achieved by loading samples into one of two short symmetric type diamond anvil cells (DACs) with either a 78° or 81° opening angle. Sample chambers of 180  $\mu$ m diameter were laser ablated into rhenium gaskets that were pre-indented to ~40  $\mu$ m thickness. For each sample, a single crystal of wadsleyite ~30  $\mu$ m in diameter was parallel-polished down to a thickness of ~10  $\pm$  2  $\mu$ m. Each sample was loaded into a DAC equipped with Boehler-Almax diamond anvils with 300  $\mu$ m culets. Two ruby spheres were placed inside each cell as pressure standards, with one ruby placed close to the center of the sample chamber to serve as the primary pressure standard and the other ruby placed near the edge of the sample chamber to monitor the possible development of pressure gradients. Ruby pressures were calculated from the shift of the  $R_1$  ruby fluorescence line using the quasi-hydrostatic calibration from Jacobsen et al. (2008). Neon was loaded using the COMPRES-GSECARS gas loading system (Rivers et al. 2008) to serve as a quasi-hydrostatic pressure-transmitting medium.

#### X-ray diffraction experiments

Single-crystal X-ray diffraction (XRD) data were collected on beamline 13-BM-C of the APS. The incident X-ray beam was monochromatized with a silicon (311) crystal to 0.434 Å incident wavelength with 1 eV energy bandwidth and focused to a 15 × 15  $\mu$ m<sup>2</sup> spot. A Pilatus 1M (Dectris) detector with 1 mm thick silicon sensor was used to record the diffraction patterns. The sample-to-detector distance and the tilt of the detector was calibrated using LaB<sub>6</sub> (Zhang et al. 2017). At each pressure, step scans were collected in steps of 1° at 1s/deg in the  $\varphi$  direction using a detector with two collecting positions. The collecting positions were moved to be positioned 20° apart in 2 $\theta$  angle. Diffraction intensity data for crystal structure refinements were collected at ambient conditions before gas loading and at each subsequent pressure step. High-pressure data were collected by compressing the DAC with a gas membrane cell at pressure intervals of 1–1.5 GPa. After increasing the pressure at each pressure step, the sample was allowed to sit for 10–15 min before data collection to stabilize the pressure. The reported pressures are the average of pressures measured before and after XRD data collection. The reported uncertainty is half of the absolute pressure difference before and after XRD collection. When this pressure difference was smaller than 0.1 GPa, 0.1 GPa was used as the pressure uncertainty to reflect the linewidth of the ruby fluorescence spectrum.

Diffraction intensities and unit cell parameters were obtained using the APEX3 software (Bruker). SHELXL (Dolomanov et al. 2009; Sheldrick 2015) with the Olex2 general user interface was used to refine the crystal structure using peak intensities reduced by the APEX3 software. All crystal structures were refined using intensity data collected from both of the collecting positions of the detector. Two models were used to refine the crystal structure: an orthorhombic (Imma) model from Jacobsen et al. (2005) and a monoclinic (I2/m) model from Smyth et al. (1997). The difference between them is that Smyth et al. (1997) splits the M3 site into two non-equivalent sites denoted M3A and M3B, and O4 site is split into O4A and O4B, where O4A is bonded to M3A and O4B bonded to M3B. Refinement parameters at each pressure step including the  $2\theta$  range, number of reflections, hkl range, and merging, and internal R-factors are listed in Tables S1 and S2.

206 Results

### Mössbauer Spectroscopy

207

208

209

210

211

212

213

214

215

216

217

218

219

220

221

222

223

224

225

226

227

228

229

230

Ambient-pressure SMS data for the more hydrous wadsleyite (Z0570) show that 24.7(1.1)% of the total Fe was Fe<sup>3+</sup> with an isomer shift of 0.082(9) mm/s and quadrupole splitting of 0.358(9) mm/s. The quadrupole splitting for Fe<sup>2+</sup> was 2.638(3) mm/s. For the less hydrous wadsleyite sample (Z0902), 12.8(1.0)% of the total Fe was Fe<sup>3+</sup> with an isomer shift of 0.106(17) mm/s and quadrupole splitting of 0.25(2) mm/s. The quadrupole splitting for the Fe<sup>2+</sup> site was 2.657(4) mm/s (Table 1). The isomer shifts (relative to stainless steel) and quadrupole splitting values reported here for Z0570 are an improvement over those measured by conventional Mössbauer spectroscopy in Chang et al. (2015) because of improved signal-to-noise ratio in the current data. Chang et al. (2015) did not measure the Fe<sup>3+</sup> content of Z0902. Combining the current SMS results with the major element analyses and water content the determinations from Chang et al. (2015),we obtain chemical formulas  $(Mg_{1.638}^{2+}Fe_{0.145}^{2+}Fe_{0.047}^{3+})H_{0.320}SiO_4$  for sample Z0570 and  $(Mg_{1.782}^{2+}Fe_{0.173}^{2+}Fe_{0.025}^{3+})H_{0.041}SiO_4$  for sample Z0902. The measured time-domain spectra and calculated energy-domain spectra of the best-fit hyperfine model are shown in Figure S2.

#### **Equations of State**

Our ambient-pressure diffraction data show that sample Z0902 (0.25 wt% H<sub>2</sub>O) has a slight monoclinic distortion, with  $\beta$  = 90.034(18)° and lattice parameters of  $a_0$  = 5.7119(5),  $b_0$  = 11.4785(5),  $c_0$  = 8.282(2), resulting in a calculated unit cell volume of 543.00(14)Å<sup>3</sup>. The more hydrous wadsleyite sample, Z0570 (2 wt% H<sub>2</sub>O), also has a slight monoclinic distortion, with  $\beta$  = 90.015(3)° and lattice parameters of  $a_0$  = 5.6965(2),  $b_0$  = 11.5431(4),  $c_0$  = 8.269(3), resulting in a calculated unit cell volume of 543.7(2) Å<sup>3</sup>. Based on these unit cell volumes and the detailed compositions given above, the reference density for the more hydrous sample Z0570 is  $\rho_0$  = 3.5064(13) g/cm<sup>3</sup>, and that for the less hydrous sample Z0902 is  $\rho_0$  = 3.584(1) g/cm<sup>3</sup>.

During compression up to about 10 GPa, the  $\beta$ -angle for both samples was essentially invariant. However, above 9 GPa, both samples exhibit a linearly increasing  $\beta$ -angle with pressure, although by markedly different amounts (Figure 1). Whereas the  $\beta$ -angle in the more hydrous sample (Z0570) only increased by about 0.1° between 10 and 30 GPa, reaching 90.09(2)° at the highest pressure of 33 GPa, the  $\beta$ -angle of the less hydrous sample (Z0902) increased by nearly 0.5°, reaching a value of 90.53(4)° at the maximum pressure of 35 GPa. The lattice parameters at each pressure refined for both orthorhombic and monoclinic symmetry for both samples are provided in Tables S3–S6.

Unit cell volumes were also calculated using both orthorhombic and monoclinic symmetry for both samples at each pressure (Tables S3-S6). We fit the pressure–volume (P-V) data to a third-order Birch-Murnaghan equation of state (BM3-EOS), where  $K_{70}$  is the reference bulk modulus at ambient pressure,  $K_{70}$  is the first pressure derivative of the bulk modulus evaluated at P=0, and  $V_0$  is the reference volume at ambient pressure. The EOS fit was performed with EOSFit7c (Angel et al. 2014). The inverse of the measurement uncertainties were used as weights for least-squares fits. The resulting EOS parameters for the more hydrous sample (Z0570) using orthorhombic symmetry are:  $V_0 = 543.19(23)$  Å $^3$ ,  $K_{70} = 164.0(2.7)$  GPa, and  $K_{70}' = 4.26(23)$ . Assuming monoclinic symmetry for Z0902 we obtain  $V_0 = 543.09(22)$  Å $^3$ ,  $K_{70} = 172.3(2.3)$  GPa, and  $K_{70}' = 3.91(15)$ . Based on statistical significance, our preferred EOS fit to the more hydrous sample (Z0570) assumes orthorhombic symmetry and monoclinic symmetry for the less hydrous sample (Z0902), which are plotted in Figure 2. EOS parameters for both compositions in both crystal systems are given in Table S7.

## **Structure Refinements**

Variation of the lattice parameters with pressure are plotted in Figure 3. A linearized third-order BM-EOS fit was used to determine the linear compressibilities along the crystal axes (Angel et al. 2014). The resulting linear moduli and axial compressibilities are given in Table S8. In both samples, the *c*-axis is the most compressible, and the *a*- and *b*-axes have about the same compressibility. However, with increased water content, the *c*-axis becomes more incompressible, while the *a*- and *b*-axes become more

compressible. We also evaluated the M–O bond lengths and polyhedral volumes as a function of pressure, which are shown in Figures S3 and S4 and listed in Table S8. Compression data of all polyhedral volumes are plotted in Figure 4.

The ambient-pressure structure refinements show vacancies only at the M3 sites, similar to what has been observed in previous studies (Smyth et al. 1994; Jacobsen et al. 2005; Holl et al. 2008; Purevjav et al. 2016). For the less hydrous and monoclinic sample (Z0902), the total site occupancies were 100% for M1, M2, and M3A, but 94.9% in M3B, indicative of strongly preferred vacancy ordering onto the M3B site, which has not previously been reported. The refined Fe occupancies at each site in Z0902 were 9.8% in M1, 3.8% in M2, 1.2% in M3A, and 9.4% in M3B. For the very hydrous sample (Z0570) we observe no vacancy ordering between M3A and M3B and used the orthorhombic symmetry, finding the total site occupancies were 100% for M1 and M2, but 87.8% in M3, consistent with there being more hydrogen-related cation vacancies in the more hydrous sample. In Z0570, we refined Fe/Mg as well and found 11.2% Fe in M1, 0.8% in M2, and 6.4% in M3.

The refined site occupancies obtained at room pressure were fixed for the high-pressure structure refinements, except for the M3 site (M3A and M3B), which contains vacancies. However, we did not observe significant changes in vacancy ordering with increasing pressure. Our results also suggest that there is no Fe<sup>3+</sup> at the T site of slightly hydrous wadsleyite, but up to 4% of the Fe cations may be at the T site of very hydrous wadsleyite, consistent with previous findings (Smyth et al. 2014).

To illustrate how hydrogen potentially affects the compressibility of O-O octahedral edges in the wadsleyite structure, we plot selected O-O distances as a function of pressure in Figure 5. A second-order BM-EOS was used to fit the data with EOSFit7c (Angel et al. 2014). In Figure 5 we also plotted prediction bands instead of confidence intervals to indicate that these are the error bars on quantities calculated from a model, in contrast to error calculated directly from experimental data. The inverse of the measurement uncertainties were used as weights in least-squares fits. The 95% prediction bands of the O1-O4 (short) and O1-O1 edges for more hydrous and less hydrous wadsleyite nearly overlap, indicating very similar compressibility. The long O1-O4 and O1-O3 edge, however, respond differently under

compression in the two samples: whereas the long O1–O4 edge is less compressible in the more hydrous wadsleyite sample (Z0570), the O1–O3 edge is less compressible in the less hydrous wadsleyite. Most notably, the longer O1–O4 edge in the more hydrous sample becomes incompressible above ~25 GPa (Figure 5), but no comparable stiffening was observed in any other O–O distances, except possibly in the O1–O3 edge of the more hydrous sample, which stiffens with a lesser degree of certainty. As stated earlier, the longer O1–O4 octahedral edge is the primary hydrogen bond in wadsleyite (Sano-Furukawa et al. 2011; Purevjav et al. 2016). A comprehensive overview of all O–O distances at the M1, M2, and M3 sites comparing both H<sub>2</sub>O compositions is given in Figure S5.

293 Discussion

### Ordering in wadsleyite

Our observation that Fe-bearing hydrous wadsleyite distorts from orthorhombic to monoclinic symmetry with an increasing  $\beta$ -angle above 9 GPa could explain earlier observations of new Raman peaks above ~9 GPa in the Raman spectra of hydrous Fe-bearing wadsleyite (Kleppe et al. 2006). Jacobsen et al. (2005) and Holl et al. (2008) found that in pure-Mg wadsleyite there is a correlation between monoclinic distortion and increasing water content. In contrast, in our Fe-bearing samples, our less hydrous sample with 0.25 wt%  $H_2O$  actually deviates more from orthorhombic symmetry than the more hydrous sample with ~2 wt%  $H_2O$ . To date, the crystal symmetry of hydrous wadsleyite has not been investigated as a function of pressure. Surprisingly, on compression above 9 GPa, the less hydrous sample deviates significantly more from orthorhombic symmetry than the more hydrous sample (Figure 1). Thus, the symmetry of Fe-bearing hydrous wadsleyite cannot be understood based on water content alone.

In the less hydrous wadsleyite sample, the M3B octahedron has a slightly larger volume than the M3A octahedron. This volume difference is related to M-site vacancies and may be caused by enhanced O-O repulsion in the absence of a central cation (Jacobsen et al. 2005). If the larger polyhedral volume of

310

311

312

313

314

315

316

317

318

319

320

321

322

323

324

325

326

327

328

329

330

331

332

333

334

the M3B site is the result of a higher vacancy concentration as compared to the M3A site, the M3B site can be expected to be more compressible, which is precisely what we observe in the polyhedral moduli (Table 2) and interatomic distances (Table S9). Due to the increased compressibility of the M3B site, at pressures exceeding 10 GPa it becomes smaller in volume than the M3A site (Table S12, S13, Figure S6), which corresponds to the pressure at which we begin seeing the more distinct symmetry change from orthorhombic to monoclinic. Orthorhombic symmetry in wadsleyite requires the plane perpendicular to the b-axis between equivalent M3 sites as a mirror plane (Smyth et al. 1997; Ye et al. 2010, 2011). At low pressure, this plane is almost perpendicular to the a-axis but slightly tilted. With increasing pressure, the volume of the M3B octahedron decreases more than that of the M3A octahedron and at around 10 GPa drops below the volume of the M3A octahedron (Table S12, S13, Figure S6), leading the (010) plane to increasingly tilt, which breaks the mirror symmetry and causes the β-angle to deviate from 90°. In short, the evolution of the  $\beta$ -angle at high pressures is likely due to the difference in vacancy population of the two non-equivalent M3 sites and their corresponding differences in polyhedral compressibility. We propose that the monoclinic distortion in wadsleyite increases with pressure when there is a significant difference in the vacancy populations or in the Mg-Fe occupancies of the M3A and M3B sites, leading to those sites having different compressibility and thus further distortion from orthorhombic symmetry. The more hydrous wadsleyite sample in our study had no significant difference in the occupancies of the M3 sites, which have similar compressibility, thus the plane perpendicular to the b-axis was retained as a mirror symmetry element Our observations of changes in the crystal symmetry at ~9 GPa may shed light on some previous spectroscopic observations. In Fe-free nominally anhydrous wadslevite, Chopelas (1991) observed seven

Our observations of changes in the crystal symmetry at ~9 GPa may shed light on some previous spectroscopic observations. In Fe-free nominally anhydrous wadsleyite, Chopelas (1991) observed seven Raman mode changes at 9.2 GPa, which the author posited as evidence of a second-order phase transition. Cynn and Hofmeister (1994) reported high-pressure infrared data for Fe-bearing wadsleyite and described a minor structure change at 9 GPa. Kleppe et al. (2006) reported the addition of four new Raman modes in the mid-frequency range at 9 GPa in hydrous Fo<sub>90</sub> wadsleyite. If the change in wadsleyite crystal symmetry to monoclinic symmetry above 9 GPa is due to the M3 and O4 sites splitting into two non-

equivalent sites, the changes in vibrational modes are likely to result from a distortion of individual octahedra since the affected vibrations are related to MgO6 octahedra. Our high-pressure structure data could therefore potentially reconcile several previously observed changes in vibrational spectra at high pressures.

### Influence of hydroxyl groups on the equation of state

The elastic moduli and their pressure derivatives are needed to calculate density and sound velocities at high pressures. For wadsleyite, previous studies have shown that the bulk modulus ( $K_0$ ) decreases with water content (e.g. Jacobsen 2005) and increases with iron content (e.g. Hazen 1993), as recently reviewed by Buchen et al. (2017) and Wang et al. (2018). In agreement with these trends, our  $K_0$  of ~164 GPa for hydrous  $Fo_{89}$  wadsleyite with 2 wt%  $H_2O$  is about 6% lower than dry  $Fo_{90}$  wadsleyite (Li and Liebermann 2000; Liu et al. 2009). The relationship between water content and the pressure derivative of the bulk modulus ( $K_0$ ) shows no obvious trend (e.g., Chang et al. 2015). Holl et al. (2008) suggested that  $K_0$ ' should increase with water content because the strong O–O repulsive forces on compression are ultimately a more important factor than the initially larger and more compressible partially vacant M sites. But experiments by Holl et al. (2008) and Chang et al. (2015) found no link between water content and  $K_0$ '. Unfortunately, attempts to resolve this discrepancy have been hampered by a range of derived values for  $K_0$ ' that can be dependent on experimental factors including data density, pressure range, pressure medium, and pressure calibration, among others.

Buchen et al. (2018) obtained  $K_{50}' = 4.13(8)$  for a slightly hydrous wadsleyite (~0.24 wt.% water) with Fo<sub>89</sub> composition using Brillouin spectroscopy, and  $K_{70}' = 4.4(2)$  on the same sample from static compression using the BM3-EOS to  $P_{\text{max}} = 20$  GPa with ruby pressures and 10 data points (Buchen et al. 2017), where the subscript S in  $K_{50}'$  refers to the adiabatic bulk modulus and the subscript T in  $K_{70}'$  refers to the isothermal bulk modulus. Mao et al. (2011) and Chang et al. (2015) both evaluated the same hydrous Fo<sub>89</sub> wadsleyite as this study (Z0570) with ~2 wt% water but Mao et al. (2011) reported  $K_{50}' = 4.8(1)$  using Brillouin spectroscopy, while Chang et al. (2015) obtained  $K_{70}' = 3.77(14)$  from static

compression using a BM3-EOS to  $P_{\text{max}} = 32$  GPa with ruby pressures and 31 data points. It should be noted, however, that Chang et al. (2015) did not have an experimental  $V_0$  value, which is an important anchor in fitting  $K_{\text{T0}}$ ' with the BM3-EOS because the derivative is effectively evaluated at zero pressure. For comparison, we found  $K_{\text{T0}}$ ' = 4.26(23) for Z0570 in this study using the BM3-EOS to  $P_{\text{max}} = 33$  GPa and 22 P-V points. Chang et al. (2015) suggested that the discrepancy in  $K_0$ ' between their study and that of Mao et al. (2011) was potentially due to the way density was estimated at high pressure by Mao et al. (2011) by iteration, potentially leading to a higher  $K_0$ '.

We examined the effects of the selection of different crystal symmetry (monoclinic versus orthorhombic) on the equations of state of wadsleyite by comparing XRD data evaluated using either orthorhombic or monoclinic symmetry. In Figure 6, we compare P-V and  $F_E-f_E$  plots of the compression data using orthorhombic symmetry versus using the observed monoclinic  $\beta$ -angles in calculating volume. The results are compiled in Tables S3–S6, and S7. When fitting our P-V data to the BM3-EOS assuming orthorhombic symmetry for the more hydrous wadsleyite (Z0570) we obtain:  $V_0 = 543.19(23)$  Å<sup>3</sup>,  $K_{T0} = 164.0(2.7)$  GPa, and  $K_{T0}' = 4.26(23)$ , whereas on using the monoclinic angles, we obtain:  $V_0 = 543.25(23)$  Å<sup>3</sup>,  $K_{T0} = 162.5(2.6)$  GPa, and  $K_{T0}' = 4.45(22)$ . In short, these EOS parameters agree within their mutual uncertainties, which is not surprising as the  $\beta$ -angle is not very distorted from 90° and the distortion only showed a quite gradual increase with pressure above 10 GPa for sample Z0570. However, with the less hydrous wadsleyite (Z0902), the BM3-EOS parameters assuming orthorhombic symmetry are:  $V_0 = 543.75(29)$  Å<sup>3</sup>,  $K_{T0} = 165.7(3.4)$  GPa, and  $K_{T0}' = 5.51(28)$ , whereas when using monoclinic symmetry and the observed monoclinic  $\beta$ -angles, we obtain:  $V_0 = 543.09(22)$  Å<sup>3</sup>,  $K_{T0} = 172.3(2.3)$  GPa, and  $K_{T0}' = 3.91(15)$ . Assuming a fixed orthorhombic symmetry at all pressures produced lower  $K_{T0}$  values, but the most pronounced effect is the higher first pressure derivative,  $K_{T0}'$ .

#### Hydrogen bonds at high pressure

The long O1–O4 edge of the M3 site is the primary location for hydrogen bonds in wadsleyite, as previously determined by neutron diffraction (Purevjav et al. 2016). While the observed incompressibility

of the long O1–O4 edge in the very hydrous sample (Z0570) above 25 GPa might be interpreted as strong hydrogen bonding, the fact that the long O1–O4 edge does not shorten below 2.90(1) Å, even up to the highest pressure (Figure S5), indicates that the long O1–O4 hydrogen-bonded edge is still far longer than what is considered strong hydrogen bonding, as defined by d(O...O) < 2.5–2.7 Å (Libowitzky 1999). In contrast, high-pressure FTIR data (Yang et al. 2014) up to ~20 GPa and high-pressure Raman data up to ~50 GPa (Kleppe et al. 2006) on hydrous wadsleyite show that the primary O–H stretching modes at 3360–3320 cm<sup>-1</sup> (at 1 atm) gradually shift to lower frequency, reaching values below ~3200 cm<sup>-1</sup> above about 20 GPa, consistent with strong hydrogen bonding (Libowitzky 1999).

The primary hydrogen bond in wadsleyite, therefore, deviates significantly from the relation between O...O distances and O–H stretching frequencies above 20 GPa (Figure 7). The simplest explanation we can propose, though not prove, involves a shift of the hydrogen atom off the longer O1–O4 edge of the M3 site either into the vacant M3 site or more along the *c*-axis above O1, either way making the O1–H...O4 hydrogen bond angle even lower than the observed angle of 171° at room pressure (Purevjav et al. 2016). If the hydrogen bond becomes more non-linear with pressure, the hydrogen atom may move further away from the donor oxygen and O–H stretching frequency may continue to drop, decoupling the O–H stretching frequency from the relation to hydrogen bond length for linear hydrogen bonds (Libowitzky 1999). Future high-pressure polarized-FTIR measurements or high-pressure neutron diffraction experiments of hydrous wadsleyite under hydrostatic compression might be performed to test this hypothesis.

407 Implications

Wadsleyite is one of the most important minerals that control the physical and chemical properties of the mantle transition zone. To better understand the effects of hydration on the physical properties of wadsleyite at the atomic scale, single-crystal X-ray structure refinements of very hydrous (2.0 wt% H<sub>2</sub>O) and slightly hydrous (0.25 wt% H<sub>2</sub>O) Fo<sub>90</sub> wadsleyite were used to evaluate the crystal structure and hydrogen bond distances up to 32 GPa.

414

415

416

417

418

419

420

421

422

423

424

425

426

427

428

429

430

431

432

433

434

435

436

437

438

At pressures exceeding 9 GPa, hydrous Fo<sub>90</sub> wadsleyite deviates from orthorhombic symmetry to have monoclinic symmetry, which we interpret as resulting from the difference in compression behavior of the split M3 site due to Mg-Fe and vacancy ordering. An increase in the β-angle of hydrous wadsleyite with pressure has implications for equation of state parameters if lattice parameters are erroneously fitted to orthorhombic symmetry. When the monoclinic symmetry is used in high-pressure EOS fits, our results suggest that  $K_{T0}$  is lowered while  $K_{T0}$  increases with hydration of wadsleyite. In wadsleyite, hydroxylation is associated with cation vacancies, and vacancies have been found to increase compressibility and  $K_{70}$  of other minerals such as spinels (Nestola et al. 2009). The demonstrated difference in calculated volume due to assumed orthorhombic symmetry, especially at P > 10 GPa where the monoclinic angle may increase, could partly explain some aspects of the controversial relationship between water content and  $K_0$ '. For example, the  $K_{70}$ ' values obtained by static compression for the same samples in this study (Z0570 and Z0902) and reported in Chang et al. (2015) assuming orthorhombic symmetry were identical and anomalously low with  $K_{T0}' = 3.7(2)$ , whereas we obtained  $K_{T0}' = 4.5(2)$  for Z0570 and  $K_{T0}' = 3.9(2)$  for Z0902. Therefore, our results show that ~2 wt% H<sub>2</sub>O decreases the bulk modulus by about ~6% and increases  $K_{T0}$ ' by about 17%. The decrease of  $K_{T0}$  and increase of  $K_{T0}$ ' can cause a volume crossover on compression (Figure 2), although the more hydrous sample remains less dense at high pressure.

The primary hydrogen bond in wadsleyite, defined by O1–H...O4 along the longer O1–O4 edge of the M3 site, becomes incompressible at pressures above 25 GPa. Although strong hydrogen bonding in wadsleyite above ~15 GPa is implied from previous spectroscopic studies showing O–H stretching frequencies that dropped below 3200 cm<sup>-1</sup> (Yang et al. 2014; Kleppe et al. 2006), we found that the hydrogen bond distance, d(O1...O4), does not drop below 2.9 Å in length and certainly not into the region of strong hydrogen bonding at 2.5–2.7 Å. We conclude that the primary hydrogen bond in wadsleyite may become more non-linear at high pressures. This is the simplest explanation for the observed combination of a long O...O distance and low O–H stretching frequency and could be explained if the hydrogen atom moves off the long O1–O4 edge into the vacant M3 site or out above O1 more along

the c-axis. Due to isotopic effects on hydrogen-bond potential energy functions (e.g. k 1974), short, strong hydrogen bonds are expected to be enriched in hydrogen versus deuterium (e.g. Kuroda et al. 1979). Even though the hydrogen-bond length in wadsleyite determined here at transition zone pressures would not predict strong isotopic fractionation ( $\delta D$ ), the observed O–H stretching frequencies below 3300 cm<sup>-1</sup> (Yang et al. 2014) indicate otherwise, highlighting the importance of combining structure (XRD) and spectroscopic evidence (e.g. Figure 7) to evaluate hydrogen-bonding geometry at pressures where neutron diffraction is not yet feasible.

## Data Availability Statement

- All structure data as .cif files have been uploaded to the American Mineralogist Crystal Structure
- 450 Database.

#### Acknowledgements

This research was supported by the US National Science Foundation (NSF) awards EAR-1853521 to S.D. Jacobsen and EAR-1725673 to E.C. Thompson. S.D.J. also acknowledges support from the Alexander von Humboldt Foundation. This work was performed at GeoSoilEnviroCARS (The University of Chicago, Sector 13), Advanced Photon Source (APS), Argonne National Laboratory. GeoSoilEnviroCARS is supported by the National Science Foundation – Earth Sciences (EAR – 1634415) and Department of Energy – GeoSciences (DE-FG02-94ER14466). This research used resources of the Advanced Photon Source, a U.S. Department of Energy (DOE) Office of Science User Facility operated for the DOE Office of Science by Argonne National Laboratory under Contract No. DE-AC02-06CH11357. Use of the COMPRES-GSECARS gas loading system was supported by COMPRES under NSF Cooperative Agreement EAR -1606856. Single-crystal diffraction experiments on beamline 13-BM-C were supported in part by the Partnership for Extreme Crystallography (PX^2) under NSF EAR-1661511. We thank

Sergey Tkachev for help with gas loading, Joseph R. Smyth for synthesis of sample Z0902, and Jiyong 465 Zhao for assistance with the SMS data collection at Sector 3 of the APS. 466 467 468 References 469 Angel, R.J., Alvaro, M., & Gonzalez-Platas, J. (2014) Eosfit7c and a Fortran module (library) for 470 equation of state calculations. Zeitschrift für Kristallographie-Crystalline Materials, 229(5), 405-471 419. https://doi.org/10.1515/zkri-2013-1711. Buchen, J., Marquardt, H., Ballaran, T.B., Kawazoe, T., & McCammon, C. (2017) The equation of state 472 473 of wadsleyite solid solutions: Constraining the effects of anisotropy and crystal 474 chemistry. American Mineralogist, 102(12), 2494-2504. https://doi.org/10.2138/am-2017-6162. 475 Buchen, J., Marquardt, H., Speziale, S., Kawazoe, T., Ballaran, T.B., & Kurnosov, A. (2018) High-476 pressure single-crystal elasticity of wadsleyite and the seismic signature of water in the shallow 477 transition zone. Earth and Planetary Science Letters, 498, 77-87. 478 https://doi.org/10.1016/j.epsl.2018.06.027. 479 Chang, Y.-Y., Jacobsen, S.D., Bina, C.R., Thomas, S.-M., Smyth, J.R., Frost, D.J., et al. (2015) 480 Comparative compressibility of hydrous wadsleyite and ringwoodite: Effect of H2O and 481 implications for detecting water in the transition zone. Journal of Geophysical Research: Solid 482 Earth, 120(12), 8259-8280. https://doi.org/10.1002/2015JB012123. 483 Chopelas, A. (1991) Thermal properties of β-Mg<sub>2</sub>SiO<sub>4</sub> at mantle pressures derived from vibrational 484 spectroscopy: Implications for the mantle at 400 km depth. Journal of Geophysical Research: 485 Solid Earth, 96(B7), 11817-11829. https://doi.org/10.1029/91JB00898. 486 Cynn, H., & Hofmeister, A.M. (1994) High pressure IR spectra of lattice modes and OH vibrations in Fe-487 bearing wadsleyite. Journal of Geophysical Research: Solid Earth, 99(B9), 17717-17727. 488 https://doi.org/10.1029/94JB01661.

489 Deon, F., Koch-Muller, M., Rhede, D., Gottschalk, M., Wirth, R., & Thomas, S.-M. (2010) Location and 490 quantification of hydroxyl in wadsleyite: New insights. American Mineralogist, 95(2-3), 312-322. 491 https://doi.org/10.2138/am.2010.3267. 492 Dolomanov, O.V., Bourhis, L.J., Gildea, R.J., Howard, J.A., & Puschmann, H. (2009) Olex2: a complete 493 structure solution, refinement and analysis program. Journal of Applied Crystallography, 42(2), 494 339-341. https://doi.org/10.1107/S0021889808042726. 495 Dong, J.J., Fischer, R.A., Stixrude, L.P., & Lithgow-Bertelloni, C.R. (2021) Constraining the volume of 496 Earth's early oceans with a temperature-dependent mantle water storage capacity model. AGU 497 Advances, 2(1), e2020AV000323. 498 Emsley, J. (1980). Very strong hydrogen bonding. Chemical Society Reviews, 9(1), 91-124. 499 Fei, H., & Katsura, T. (2020) High water solubility of ringwoodite at mantle transition zone 500 temperature. Earth and Planetary Science Letters, 531, 115987. 501 https://doi.org/10.1016/j.epsl.2019.115987. 502 Gwanmesia, G.D., Whitaker, M.L., Dai, L., James, A., Chen, H., Triplett, R.S., & Cai, N. (2020) The 503 Elastic Properties of β-Mg<sub>2</sub>SiO<sub>4</sub> Containing 0.73 wt.% of H<sub>2</sub>O to 10 GPa and 600 K by Ultrasonic 504 Interferometry with Synchrotron X-Radiation. Minerals, 10(3), 209. 505 https://doi.org/10.3390/min10030209. 506 Hazen, R.M. (1993) Comparative compressibilities of silicate spinels: anomalous behavior of (Mg, 507 Fe)<sub>2</sub>SiO<sub>4</sub>. Science, 259(5092), 206-209. https://doi.10.1126/science.259.5092.2. 508 Hazen, R.M., Weinberger, M.B., Yang, H., & Prewitt, C.T. (2000) Comparative high-pressure crystal 509 chemistry of wadslevite, β-(Mg<sub>1-x</sub>Fe<sub>x</sub>)<sub>2</sub>SiO<sub>4</sub>, with x=0 and 0.25. American Mineralogist, 85(5-6), 510 770-777. https://doi.org/10.2138/am-2000-5-617. 511 Holl, C.M., Smyth, J.R., Jacobsen, S.D., & Frost, D.J. (2008) Effects of hydration on the structure and 512 wadsleyite,  $\beta$ -Mg<sub>2</sub>SiO<sub>4</sub>. compressibility of American Mineralogist, 93(4), 598-607. 513 https://doi.org/10.2138/am.2008.2620.

514 Horiuchi, H., & Sawamoto, H. (1981). β-Mg2SiO4: Single-crystal X-ray diffraction study. American 515 Mineralogist, 66(5-6), 568-575. 516 Jacobsen, S.D., Smyth, J.R., Swope, R.J., & Sheldon, R.I. (2000) Two proton positions in the very strong 517 hydrogen bond of serandite, NaMn<sub>2</sub> [Si<sub>3</sub>O<sub>8</sub> (OH)]. American Mineralogist, 85(5-6), 745-752. 518 https://doi.org/10.2138/am-2000-5-613. 519 Jacobsen, S.D., Demouchy, S., Frost, D.J., Ballaran, T.B., & Kung, J. (2005) A systematic study of OH in 520 hydrous wadsleyite from polarized FTIR spectroscopy and single-crystal X-ray diffraction: 521 Oxygen sites for hydrogen storage in Earth's interior. American Mineralogist, 90(1), 61-70. 522 https://doi.org/10.2138/am.2005.1624. 523 Jacobsen, S.D., Holl, C.M., Adams, K.A., Fischer, R.A., Martin, E.S., Bina, C.R., et al. (2008) 524 Compression of single-crystal magnesium oxide to 118 GPa and a ruby pressure gauge for helium 525 pressure media. American Mineralogist, 93(11-12), 1823-1828. 526 https://doi.org/10.2138/am.2008.2988. 527 Karato, S.I. (2011) Water distribution across the mantle transition zone and its implications for global 528 material circulation. Earth and Planetary Science Letters, 301(3-4),413-423. 529 https://doi.org/10.1016/j.epsl.2010.11.038. 530 Kleppe, A., Jephcoat, A., Olijnyk, H., Slesinger, A., Kohn, S., & Wood, B. (2001) Raman spectroscopic 531 study of hydrous wadslevite (β-Mg<sub>2</sub>SiO<sub>4</sub>) to 50 GPa. Physics and Chemistry of Minerals, 28(4), 532 232-241. https://doi.org/10.1007/s002690100152. 533 Kleppe, A.K., Jephcoat, A.P., & Smyth, J.R. (2006) High-pressure Raman spectroscopic study of Fo<sub>90</sub> 534 hydrous wadsleyite. Physics and Chemistry of Minerals, 32(10),700-709. 535 https://doi.org/10.1007/s00269-005-0048-8. 536 Kohn, S., Brooker, R.A., Frost, D.J., Slesinger, A., & Wood, B. (2002) Ordering of hydroxyl defects in 537 hydrous wadsleyite Mineralogist, 87(2-3),  $(\beta-Mg_2SiO_4)$ . American 293-301. 538 https://doi.org/10.2138/am-2002-2-310.

- Kuroda, Y., Suzuoki, T., & Matsuo, S. (1979) The lowest  $\delta D$  value found in a hydrous silicate, pectolite.
- 540 Nature, 279, 227-228. https://doi.org/10.1038/279227a0.
- 541 Li, B., & Liebermann, R.C. (2000) Sound velocities of wadsleyite β-(Mg<sub>0.88</sub>Fe<sub>0.12</sub>) <sub>2</sub>SiO<sub>4</sub> to 10
- GPa. American Mineralogist, 85(2), 292-295. https://doi.org/10.2138/am-2000-2-305
- 543 Libowitzky, E. (1999) Correlation of OH stretching frequencies and OH...O hydrogen bond lengths in
- minerals. Monatshefte für Chemie/Chemical Monthly, 130(8), 1047-1059.
- 545 <u>https://doi.org/10.1007/BF03354882.</u>
- Liu, W., Kung, J., Li, B., Nishiyama, N., & Wang, Y. (2009). Elasticity of (Mg<sub>0.87</sub>Fe<sub>0.13</sub>) <sub>2</sub>SiO<sub>4</sub> wadsleyite
- to 12 GPa and 1073 K. Physics of the Earth and Planetary Interiors, 174(1-4), 98-104.
- 548 <u>https://doi.org/10.1016/j.pepi.2008.10.020</u>.
- 549 Mao, Z., Jacobsen, S.D., Frost, D.J., McCammon, C.A., Hauri, E.H., & Duffy, T.S. (2011) Effect of
- 550 hydration on the single-crystal elasticity of Fe-bearing wadsleyite to 12 GPa. American
- 551 Mineralogist, 96(10), 1606-1612. https://doi.org/10.2138/am.2011.3807.
- 552 McMillan, P.F., Akaogi, M., Sato, R.K., Poe, B., & Foley, J. (1991) Hydroxyl groups in β-Mg<sub>2</sub>SiO<sub>4</sub>.
- 553 American Mineralogist, 76(3-4), 354-360.
- 554 Momma, K., & Izumi, F. (2011) VESTA 3 for three-dimensional visualization of crystal, volumetric and
- 555 morphology data. Journal of applied crystallography, 44(6), 1272-1276.
- 556 https://doi.org/10.1107/S0021889811038970.
- 557 Novak A. (1974) Hydrogen bonding in solids correlation of spectroscopic and crystallographic data.
- 558 InLarge Molecules (pp. 177-216). Springer, Berlin, Heidelberg.
- Nestola, F., Smyth, J.R., Parisatto, M., Secco, L., Princivalle, F., Bruno, M., Prencipe, M., & Dal Negro,
- A. (2009) Effects of non-stoichiometry on the spinel structure at high pressure: Implications for
- Earth's mantle mineralogy. Geochimica et Cosmochimica Acta, 73(2), 489-492.
- 562 https://doi:10.1016/j.gca.2008.11.001.
- 563 Pearson, D., Brenker, F., Nestola, F., McNeill, J., Nasdala, L., Hutchison, M., et al. (2014) Hydrous
- mantle transition zone indicated by ringwoodite included within diamond. Nature 507(7491), 221.

565 https://doi.org/10.1038/nature13080. 566 Purevjav, N., Okuchi, T., Tomioka, N., Wang, X., & Hoffmann, C. (2016) Quantitative analysis of 567 hydrogen sites and occupancy in deep mantle hydrous wadsleyite using single crystal neutron 568 diffraction. Scientific Reports, 6, 34988. https://doi.org/10.1038/srep34988. 569 Rivers, M., Prakapenka, V.B., Kubo, A., Pullins, C., Holl, C.M., & Jacobsen, S.D. (2008) The 570 COMPRES/GSECARS gas-loading system for diamond anvil cells at the Advanced Photon 571 Source. High Pressure Research, 28(3), 273-292. https://doi: 10.1080/08957950802333593. 572 Sano-Furukawa, A., Kuribayashi, T., Komatsu, K., Yagi, T., & Ohtani, E. (2011) Investigation of 573 hydrogen sites of wadsleyite: A neutron diffraction study. Physics of the Earth and Planetary 574 Interiors, 189(1-2), 56-62. https://doi.org/10.1016/j.pepi.2011.07.003. 575 Sheldrick, G.M. (2015) Crystal structure refinement with SHELXL. Acta Crystallographica Section C: 576 Structural Chemistry, 71(1), 3-8. <a href="https://doi.org/10.1107/S2053229614024218">https://doi.org/10.1107/S2053229614024218</a>. 577 Smyth, J.R. (1987) β-Mg<sub>2</sub>SiO<sub>4</sub>; a potential host for water in the mantle? American Mineralogist, 72(11-578 12), 1051-1055. 579 Smyth, J.R. (1994) A crystallographic model for hydrous wadslevite (β-Mg2SiO4): an ocean in the 580 Earth's interior? American Mineralogist 79(9-10), 1021-1024. 581 Smyth, J.R., Kawamoto, T., Jacobsen, S.D., Swope, R.J., Hervig, R.L., & Holloway, J.R. (1997) Crystal 582 structure of monoclinic hydrous wadsleyite [β-(Mg,Fe)<sub>2</sub>SiO<sub>4</sub>]. American Mineralogist, 82(3-4), 583 270-275. https://doi.org/10.2138/am-1997-3-404. 584 Smyth, J.R., Bolfan-Casanova, N., Avignant, D., El-Ghozzi, M., & Hirner, S.M. (2014) Tetrahedral ferric 585 iron in oxidized hydrous wadslevite. American Mineralogist, 99(2-3), 458-466. 586 https://doi.org/10.2138/am.2014.4520. 587 Sturhahn, W. (2000) CONUSS and PHOENIX: Evaluation of nuclear resonant scattering data. Hyperfine 588 Interactions, 125(1-4), 149-172. <a href="https://doi.org/10.1023/A:1012681503686">https://doi.org/10.1023/A:1012681503686</a>.

589 Tsuchiya, J., & Tsuchiya, T. (2009). First principles investigation of the structural and elastic properties 590 of hydrous wadsleyite under pressure. Journal of Geophysical Research: Solid Earth, 114(B2). 591 https://doi.org/10.1029/2008JB005841. 592 Toellner, T.S., 2000. Monochromatization of synchrotron radiation for nuclear resonant scattering 593 experiments. Hyperfine Interactions. 125, 3-28. https://doi.org/10.1023/A:1012621317798 594 Wang, F., Barklage, M., Lou, X., van der Lee, S., Bina, C.R., & Jacobsen, S.D. (2018) HyMaTZ: A 595 Python program for modeling seismic velocities in hydrous regions of the mantle transition 596 2308-2324. zone. Geochemistry, Geophysics, Geosystems, 19(8), 597 https://doi.org/10.1029/2018GC007464. 598 Yang, X., Keppler, H., Dubrovinsky, L., & Kurnosov, A. (2014) In-situ infrared spectra of hydroxyl in 599 wadsleyite and ringwoodite at high pressure and high temperature. American Mineralogist, 99(4), 600 724–729. https://doi.org/10.2138/am.2014.4634. 601 Ye, Y., Smyth, J.R., Hushur, A., Manghnani, M.H., Lonappan, D., Dera, P., & Frost, D.J. (2010) Crystal 602 structure of hydrous wadsleyite with 2.8% H<sub>2</sub>O and compressibility to 60 GPa. American 603 Mineralogist, 95(1112), 1765-1772. https://doi.org/10.2138/am.2010.3533. 604 Ye, Y., Smyth, J.R., & Frost, D.J. (2011) Structural study of the coherent dehydration of 605 wadsleyite. American Mineralogist, 96(11-12), 1760-1767. 606 https://doi.org/10.2138/am.2011.3852. 607 Zhang, D., Dera, P.K., Eng, P.J., Stubbs, J.E., Zhang, J.S., Prakapenka, V.B., & Rivers, M.L. (2017) High 608 pressure single crystal diffraction at PX<sup>2</sup>. JoVE (Journal of Visualized Experiments), e54660. 609 https://doi: 10.3791/54660. 610

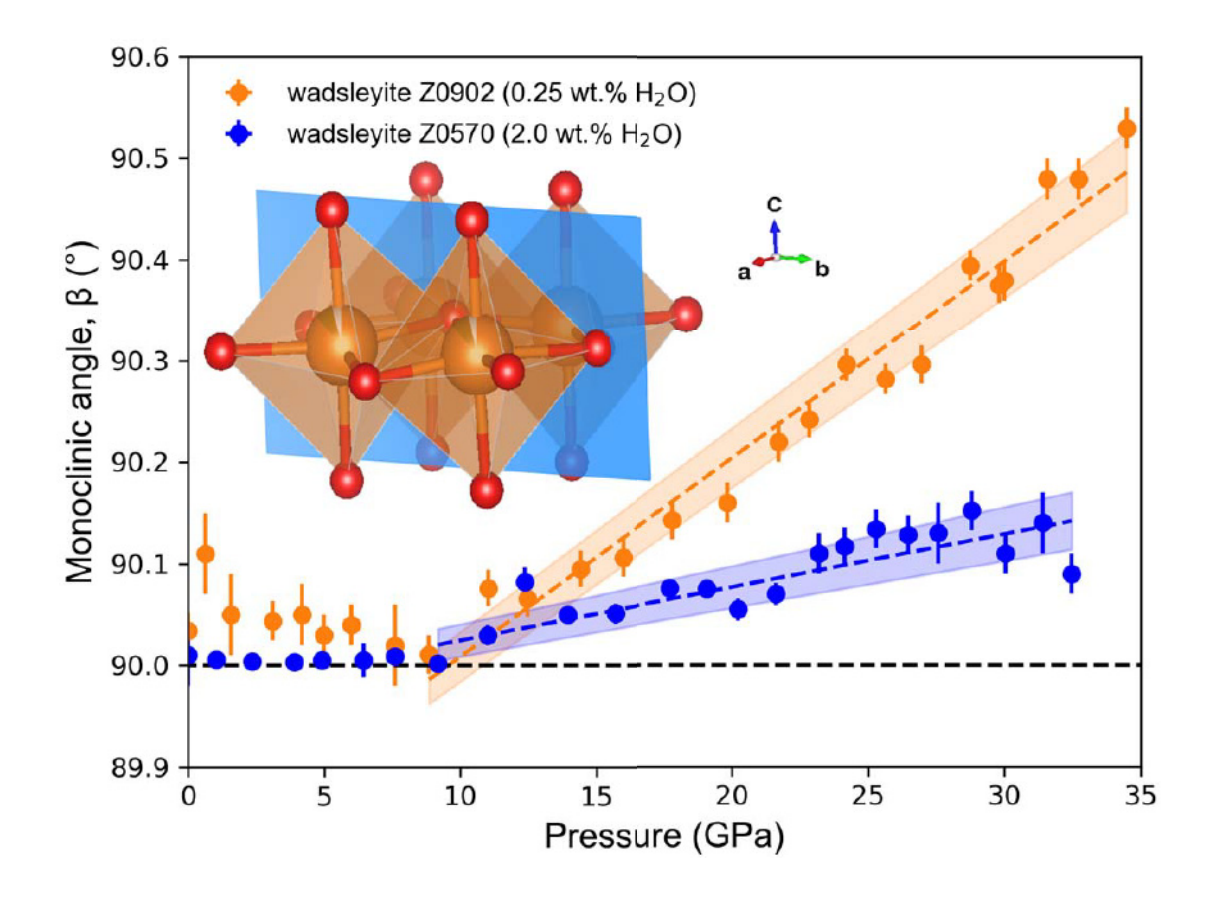


**Figure 1.** Monoclinic  $\beta$ -angle versus pressure of hydrous wadsleyite. Orange and blue dashed lines are linear fits to the data above 9 GPa for Z0902 and Z0570, respectively. The colored shaded regions indicate the 95% prediction bands. The black dashed line indicates the β-angle of the orthorhombic structure. The inset shows the local structure around the M3 octahedral site, wherein the blue plane indicates the mirror plane perpendicular to the *a*-axis for orthorhombic symmetry. The mirror plane is lost when vacancy ordering splits the M3 site into the non-equivalent M3A and M3B sites.

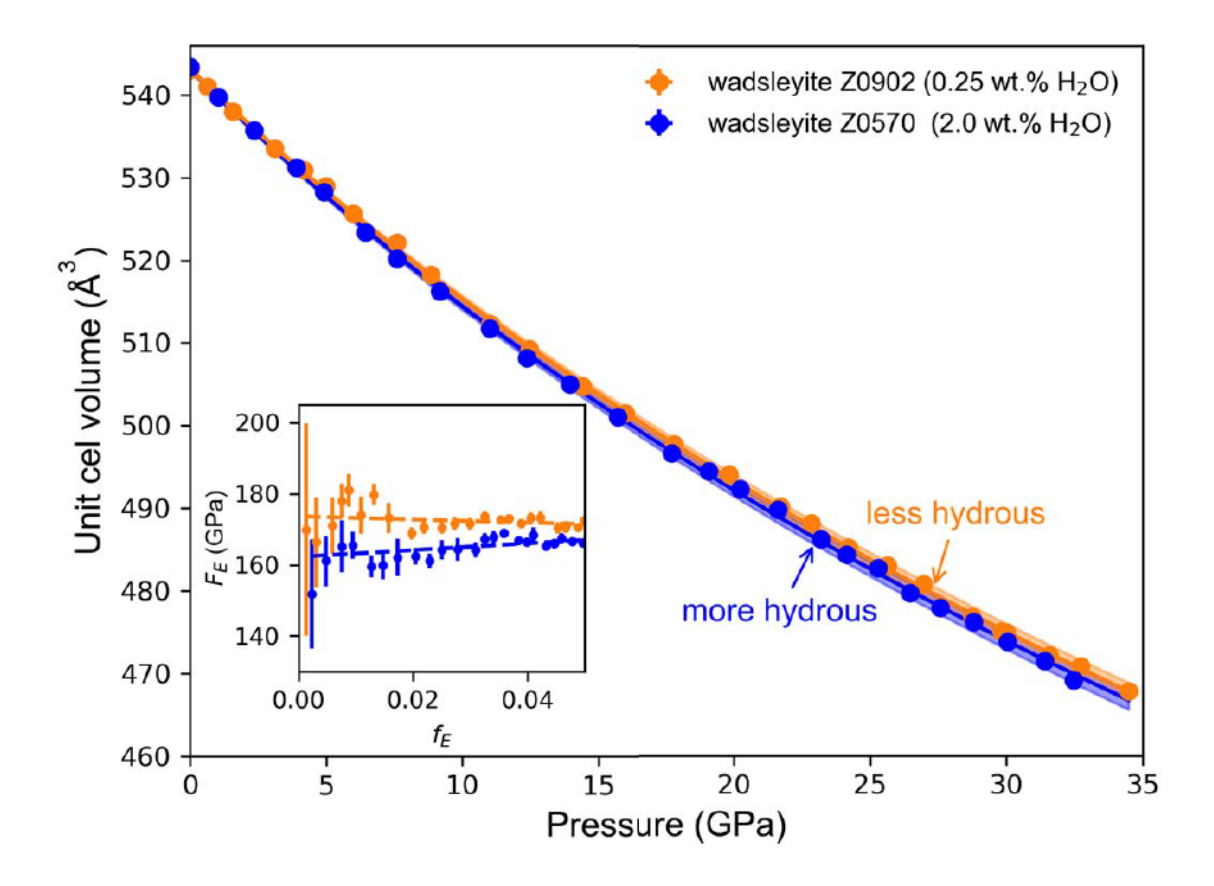


**Figure 2.** Unit cell volume *versus* pressure data for hydrous Fe-bearing wadsleyite. Fitted third-order BM-EOS are shown as solid curves. The blue and orange shaded regions show the 95% prediction band. The inset shows normalized pressure ( $F_E$ ) versus Eulerian strain ( $f_E$ ).

619

620

621

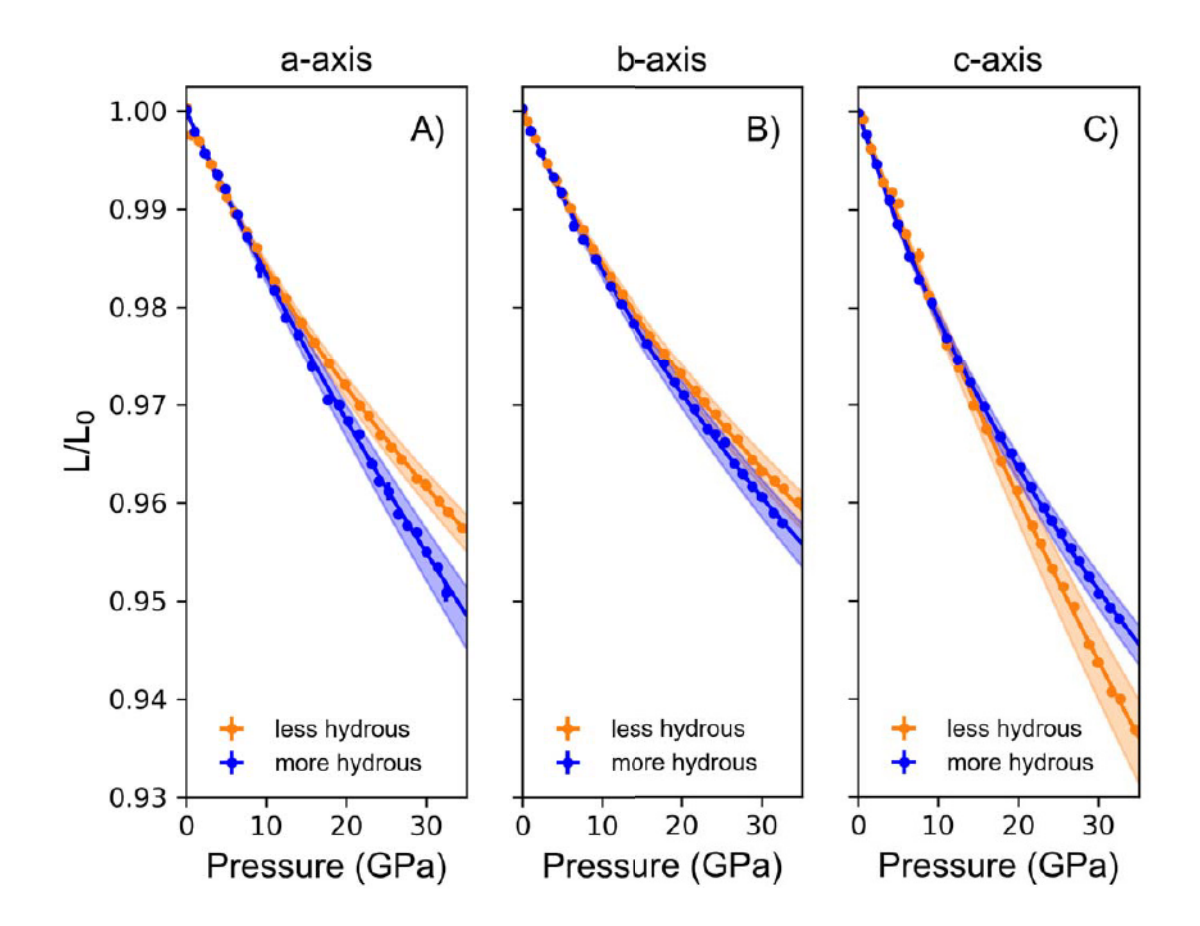


Figure 3. Axial compressibility of wadsleyite sample Z0570 with 2.0 wt%  $H_2O$  (blue data) and sample Z0902 with 0.25 wt%  $H_2O$  (orange data). Fitted third-order BM-EOS fits are shown as solid curves. The shaded regions show the 95% prediction band.

624

625

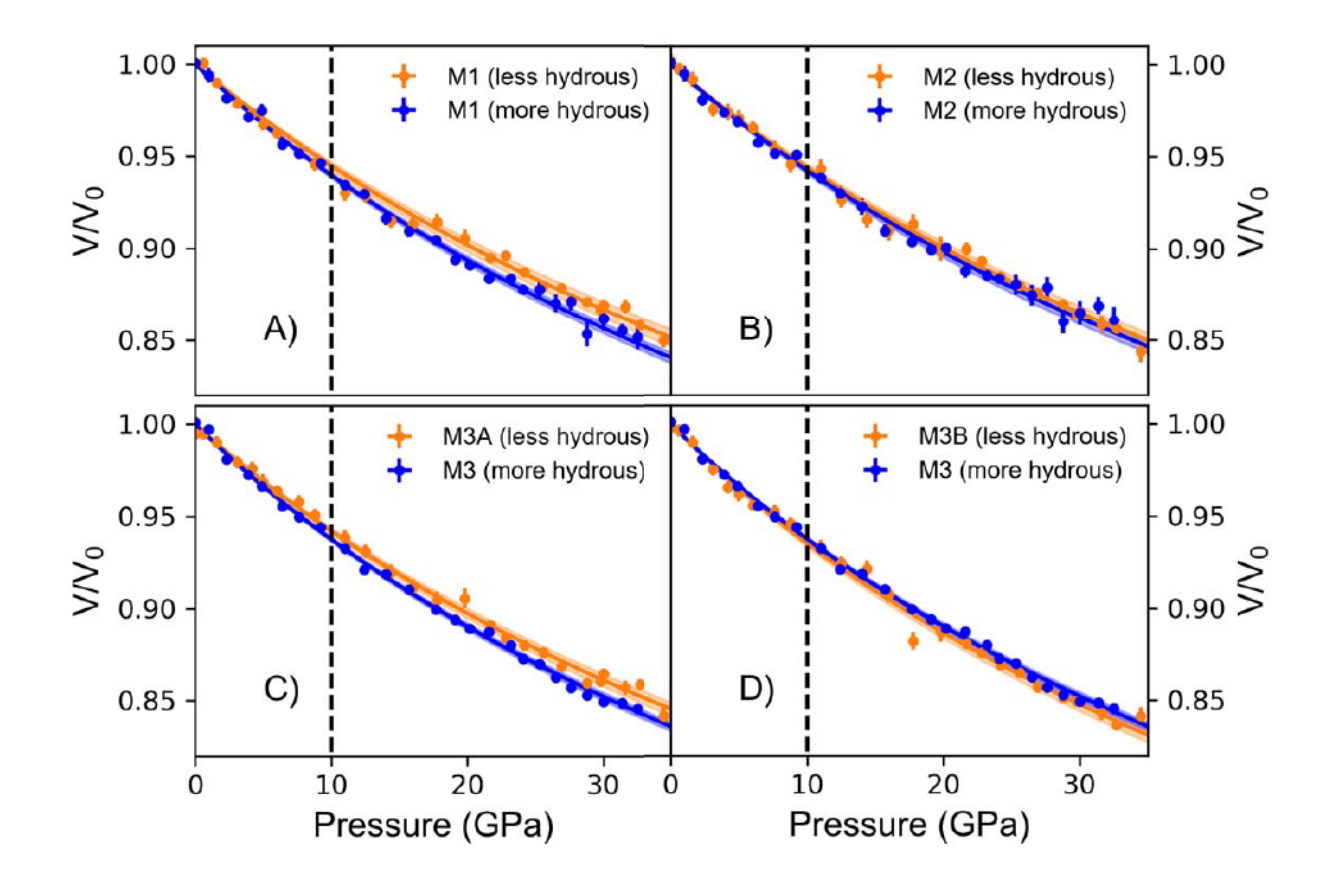
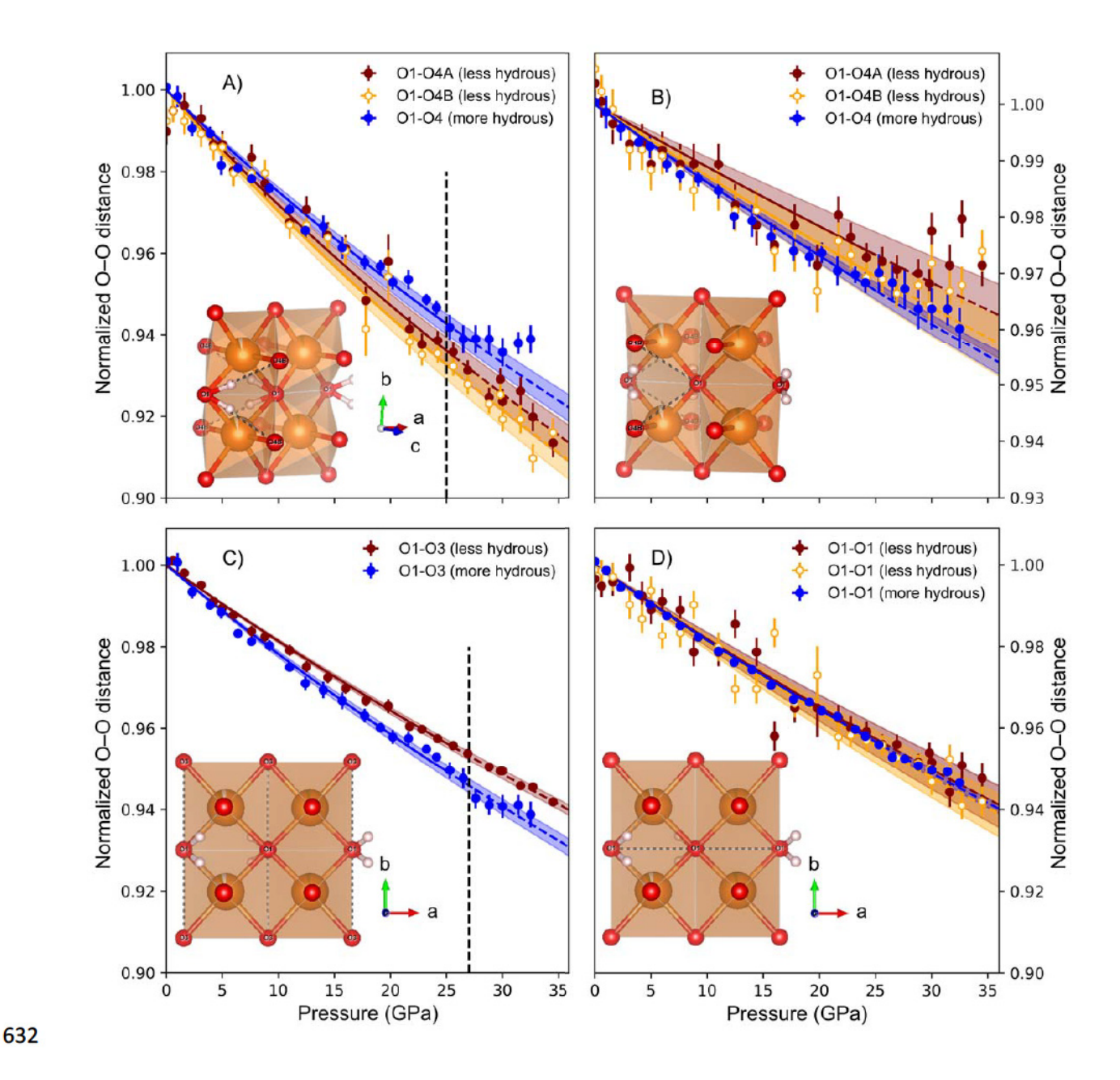


Figure 4. Octahedral volume compression of the A) M1, B) M2 and C) and D) M3 sites of hydrous wadsleyite sample Z0570 with 2.0 wt%  $H_2O$  (blue) and sample Z0902 with 0.25 wt%  $H_2O$  (orange). Solid lines show the fitted second-order BM-EOS. The shaded regions show the 95% prediction band. Dashed lines indicate the pressure at which the structure distorts from orthorhombic to monoclinic symmetry.

628

629

630



**Figure 5.** Compression of selected O...O interatomic distances in hydrous wadsleyite. A) The primary hydrogen bond: in red and orange, long O1–O4 edges on the M3A and M3B sites for sample Z0902 with 0.25 wt% H<sub>2</sub>O and monoclinic crystal symmetry. In blue, long O1–O4 edge on the M3 site in sample Z0570 with 2.0 wt% H<sub>2</sub>O and orthorhombic crystal symmetry. The dashed vertical line shows the pressure above which the long O1–O4 edge of the M3 site stops shortening above ~25 GPa. B) Same as panel A) but showing the short O1–O4 edges of the M3 sites. C) Other possible hydrogen bonds: O1–O3

634

635

636

637

of Z0902 and Z0570, with a dashed vertical line to show the pressure above which a possible change in the O1–O3 compression occurs; D) O1–O1 of Z0902 and Z0570. The distances are normalized to the distance at ambient pressure. Lines show the fitted second-order BM-EOS. Shaded regions show the 95% prediction band. The insets show where the various O–O edges are located in the crystal structure.

647

648

649

650

651

**Figure 6.** Unit cell volume versus pressure data of (A) more hydrous wadsleyite (Z0570, 2.0 wt% H<sub>2</sub>O), and (B) less hydrous wadsleyite (Z0902, 0.25 wt% H<sub>2</sub>O) in both orthorhombic (red) and monoclinic symmetries (green) with solid lines showing the fitted third order BM-EOS. Panels (C) and (D) show the corresponding normalized pressure (F<sub>E</sub>) *versus* Eulerian strain (f<sub>E</sub>), where the symmetry is either orthorhombic (red) or monoclinic (green).

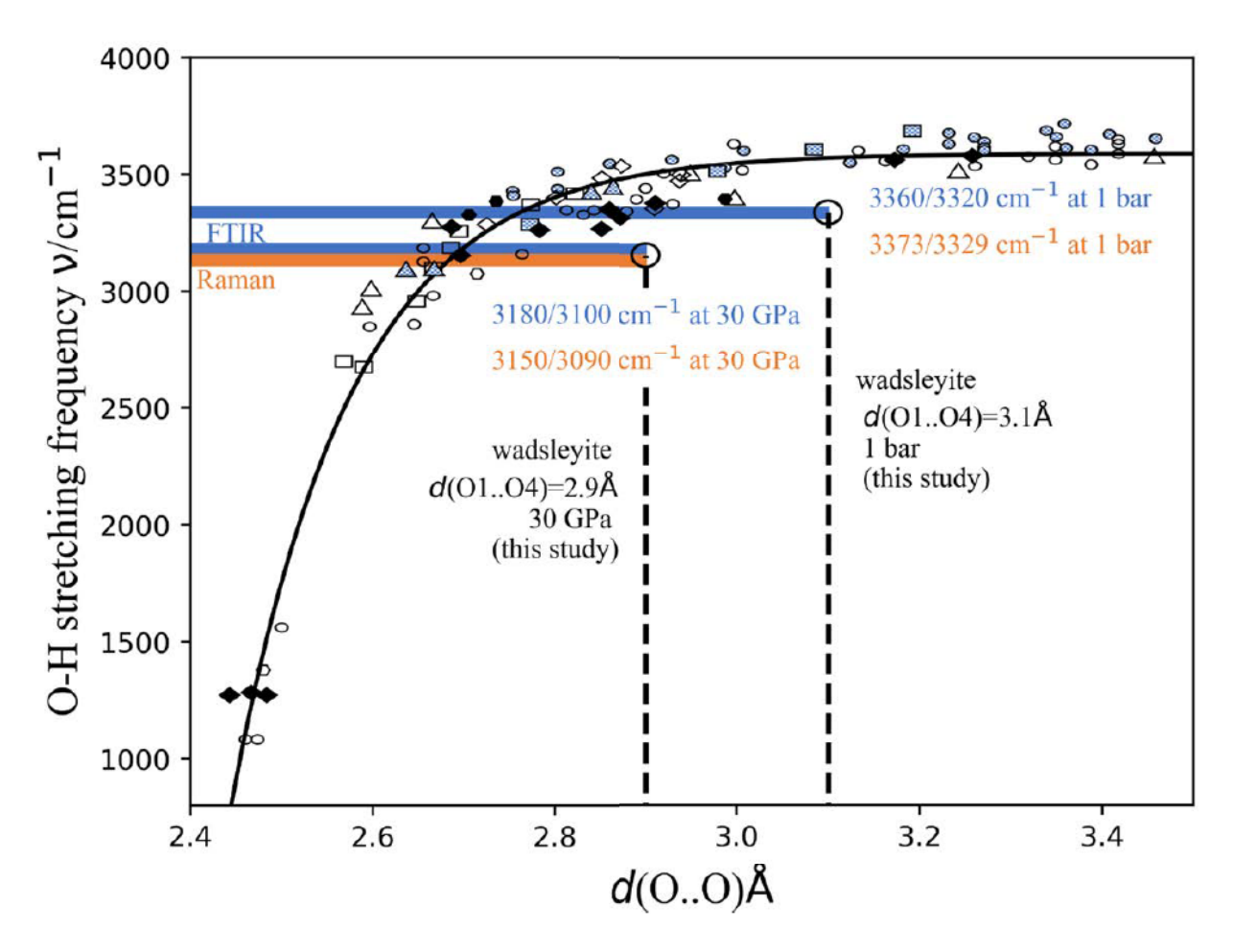


**Figure 7.** Compilation of hydrogen bond distances, d(O...O), versus O–H stretching frequencies for nearly linear hydrogen bonds in minerals, modified from Libowitzky (1999). Large circles indicate the intersection of measured d(O...O) for the O1–H...O4 hydrogen bond in wadsleyite from this study with measured spectroscopic O–H stretching frequencies from FTIR (Yang et al. 2014) and Raman studies (Kleppe et al. 2006). The FTIR O–H stretching frequencies of 3360 and 3320 cm<sup>-1</sup> at 1 bar are from Yang et al. (2014), and at 30 GPa (blue band) they are calculated from the polynomial fits published by Yang et al. (2014) from data up to 20 GPa. The Raman O–H stretching frequencies at 30 GPa of 3090 and 3150 cm<sup>-1</sup> are from the study of Kleppe et al. (2006).

# **Table 1.** Comparison of hyperfine parameters of the two wadsleyite samples.

663

664

665

666

667

	Sample	Sample	
	Z0570	Z0902	
$\mathrm{Fe}^{3^+}\!/\Sigma\mathrm{Fe}$	24.7(1.1)%	12.8(1.0)%	
Fe <sup>2+</sup> isomer shift (mm/s)	1.04	1.04	
Fe <sup>3+</sup> isomer shift (mm/s)	0.082(9)	0.106(17)	
Fe <sup>2+</sup> quadrupole splitting	2.638(3)	2.657(4)	
(mm/s)			
Fe <sup>3+</sup> quadrupole splitting	0.358(9)	0.252(20)	
(mm/s)			

**Table 2.** Compressibility of the coordination polyhedra of wadsleyite with 2.0 wt%  $H_2O$  (Z0570) and with 0.25 wt%  $H_2O$  (Z0902).

Sample	M1 (GPa)	M2 (GPa)	M3 (GPa)	M3A (GPa)	M3B (GPa)	T (GPa)
Z0570	142(1.9)	150.7(2.4)	134.2(1.5)			314(10)
Z0902	154(3.5)	152.5(3.2)		145.9(3.2)	130.3(2.6)	316(13)